# Subterahertz Phonon Dynamics in Acoustic Nanocavities

A. Huynh,[1] N. D. Lanzillotti-Kimura,[1,2] B. Jusserand,[1] B. Perrin,[1] A. Fainstein,[2]
M. F. Pascual-Winter,[1,2] E. Peronne,[1] and A. Lemaître[3]

[1]*Institut des Nanosciences de Paris, CNRS, Universités Paris 6 et 7, Campus Boucicaut, 140 rue de Lourmel, 75015 Paris, France*
[2]*Centro Atómico Bariloche and Instituto Balseiro, C.N.E.A., 8400 San Carlos de Bariloche, R.N., Argentina*
[3]*Laboratoire de Photonique et de Nanostructures, CNRS, Route de Nozay, 91460 Marcoussis, France*

(Received 26 April 2006; published 13 September 2006)

We report a direct determination of the dynamic behavior of confined acoustic phonons in nanocavities by picosecond acoustics. We provide the broadband, high resolution transmission amplitude curve in the subterahertz range, and we give evidence of resonant transmission peaks in three successive stop bands, in quantitative agreement with acoustic simulations. We furthermore demonstrate transit times in the nanosecond range at the cavity peaks reflecting the strong confinement of resonant phonons within the cavity layer. On the other hand, picosecond transit times are measured in the stop band, shorter than in any of the constituting materials, a tunneling effect well known both in photonic crystals and in macroscopic phononic systems.

DOI: 10.1103/PhysRevLett.97.115502 PACS numbers: 63.22.+m, 78.47.+p, 78.67.Pt, 43.38.+n

Acoustic phonons manifest themselves practically in all electronic, thermal, and optical phenomena in semiconductor nanostructures. Following several proposals that the modification of the acoustic phonon spectrum due to spatial confinement in standard nanostructures should strongly influence the electron-phonon interaction in these devices, it has been finally demonstrated [1] that the phonon scattering rate cannot be significantly modified by these means. Based on the concept of photon microcavity, it has been recently suggested that confining gigahertz-terahertz acoustic phonons in specifically designed resonant multilayers could significantly modify the electron-phonon interaction in nanostructures. GaAs/AlAs acoustic nanocavities have been proposed and phonon confinement demonstrated by Raman scattering [2]. The formal equivalence between the equations describing light and sound propagation has been the basis for the conception of 1D [3,4], 2D [5], and 3D [6] phononic crystals in which the acoustic impedance is artificially modulated as the refractive index is in photonic crystals. Practical demonstrations of this concept have been obtained in macroscopic crystals with spectral modifications of ultrasound in the kilohertz [4] and the megahertz range [5,6]. Such model systems, in which coherent wave experiments can be much more easily performed than in photonic devices, have been successfully used to explore basic properties of wave propagation in highly dispersive media, such as tunneling times in single [6] or multiple [4,7] phonon barriers. Macroscopic phononic crystals have potential applications in soundproof devices, but modified interactions between ultrasound and light or electrons can hardly be foreseen in such materials.

The epitaxial growth of semiconductor multilayers allows the conception of monolithic 1D phononic crystals based on the contrasting acoustic impedances of standard semiconductors such as GaAs and AlAs [3,8]. Superlattices are well known for their novel optical and electronic properties and much less as high reflectance phonon Bragg mirrors in the gigahertz-terahertz range, i.e., in the energy range which is important for the performance of several electronic and optoelectronic devices. We recently reported [2] the spectroscopic demonstration that monochromatic acoustic phonons around 0.5 THz are strongly confined in a nanometer thick GaAs layer embedded at the center of a phonon nanocavity, as photons are in optical microcavities. We present in this Letter the direct measurement of phonon spectral transmission through a similar phonon nanocavity, based on the picosecond acoustics technique [9,10]. The state of the art control of individual epitaxial layers should allow the observation of coherent phonon transmission in nanodevices working in the terahertz range. However, we demonstrate here the validity of the concept in the 100 GHz range, which well fits the performance of the presently available broadband directional transducers made of metallic layers. We demonstrate that inserting a phonon cavity between two identical phonon mirrors induces a narrow transmission peak within the lowest stop bands and that a narrow phonon wave packet centered at this peak is significantly delayed when transmitted through the device. When centered within the stop bands, the pulse becomes ''supersonic''; i.e., its velocity becomes higher than the sound velocity in any of the constituting materials of the structure. This is equivalent to ''superluminal transit'' used in the context of photon tunneling [11].

We show in Fig. 1 the structure of the GaAs/AlAs phonon devices, grown by molecular beam epitaxy on (001) oriented two-side polished GaAs substrates. The structures contain two high reflectance phonon Bragg mirrors made of 10 periods of $(3\lambda_1/4, \lambda_2/4)$ building blocks, where $\lambda_i = 47.26$ and 56.48 nm for GaAs and AlAs, respectively. The high reflectance of these mirrors is based on the acoustic impedance contrast

 

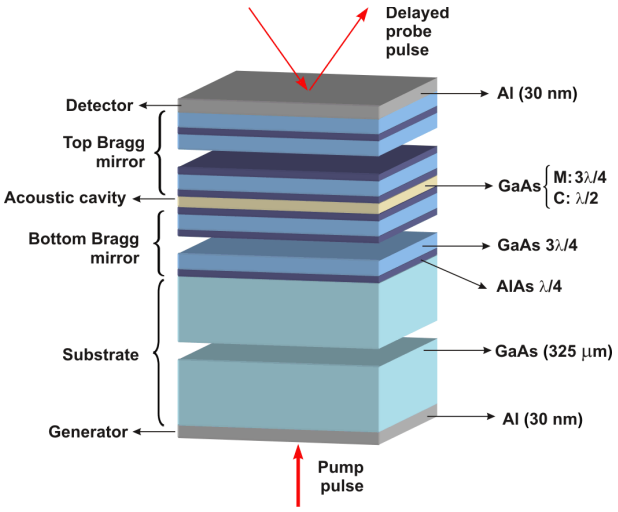


FIG. 1 (color online). Scheme of the acoustic nanodevice and configuration of the picosecond acoustic measurement.

$\varepsilon = (\rho_2 v_2 - \rho_1 v_1)/(\rho_1 v_1 \rho_2 v_2)^{1/2} \cong 0.18$, where $\rho_1$, $v_1$, $\rho_2$, and $v_2$ are the mass density and the sound velocity of GaAs and AlAs, respectively. Acoustic gaps are expected to open at integer multiples of 50 GHz. A GaAs single layer was inserted between these two mirrors, and we compare in this Letter the results on two different samples, differing only in the thickness of this layer: $3\lambda/4$ in sample $M$ and $\lambda/2$ in sample $C$. Sample $M$ (for mirror) is a standard superlattice with 20 periods, while sample $C$ is a phonon cavity. Note that terahertz phonon nanocavities are much more compact than photonic microcavities due to the shorter wavelength of acoustic waves. Broadband acoustic transmission spectroscopy [9,10,12] has been performed using thin aluminum layers deposited on both sides of the samples for generation (substrate side) and detection (surface side) of the acoustic pulse (see Fig. 1). Two hundred femtosecond optical pulses centered at 800 nm are sent at a 79 MHz repetition rate on the substrate side with a typical energy of 8 nJ/pulse focused over a 60 $\mu$m wide spot. The short absorption length in Al leads to the generation of an acoustic pulse containing frequencies up to 0.25 THz. The width of the aluminum layers has been optimized at 30 nm so that the direct interaction between light and the semiconductor is negligible in both the generation and detection processes. The sample is cooled down to 15 K so that the acoustic pulse propagates with negligible attenuation over the 325 $\mu$m thick GaAs substrate. We finally used a Sagnac interferometer [12] and a lock-in detection to measure the time variation of the imaginary part $B(t)$ of the complex optical reflectivity of the device surface, $\Delta R/R = A(t) + iB(t)$. The quantity $B(t)$ mainly reflects the displacement of the sample surface.

The interaction of the acoustic pulse with the phonon mirror and cavity is illustrated in Fig. 2. This figure shows calculations based on the transfer matrix method, in which

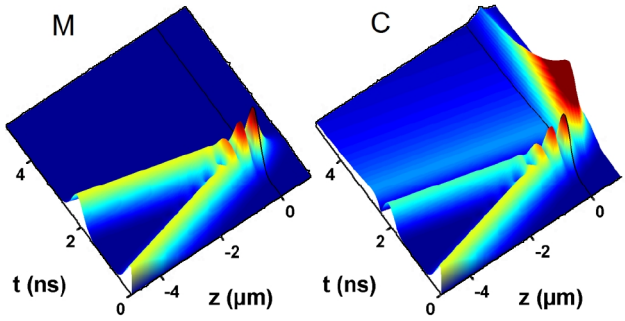


FIG. 2 (color online). Time dependence of the acoustic displacement across the device shown for sample $M$ on the left and $C$ on the right after a Gaussian pulse centered at 100 GHz with a full width of 0.2 GHz is sent from the substrate into the device. The thick black line at position $z = 0$ indicates the substrate-device interface.

a Gaussian pulse centered at 100 GHz with a full width of 0.2 GHz is sent towards the back interface. The energy distribution of the pulse is centered at the stop band of the mirror and at the cavity mode in the cavity device. For the mirror, all of the acoustic intensity is rapidly reflected towards the substrate, while, for the cavity, a significant part of the energy is transferred to the cavity mode, setting on a confined displacement that then decays slowly with time. We present in Fig. 3(a) the time evolution of the measured signal $B(t)$ in sample $C$. It is completely free of nonvibrational contributions, in contrast to similar experiments with pump and probe focused on the same side of the

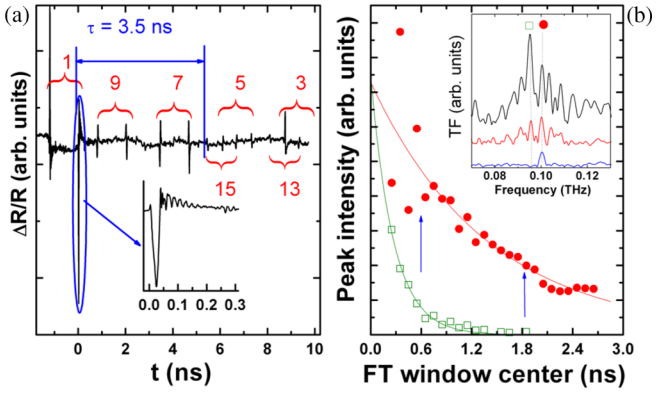


FIG. 3 (color online). (a) Imaginary part of the time resolved reflectivity on sample $C$. The brackets indicate successive pairs of echoes and the labels give the associated number of substrate traversals $(2n + 1)$. The vertical lines define the time window used for the data analysis and the inset magnifies the short time variation inside the ellipse. (b) Variation of the peak intensity at the cavity mode (solid circles) and the stop-band low energy edge (open squares) in partial FT windows with a constant length 500 ps and varying central time delays given in the abscissa. The arrows indicate the arrival of new echoes. The solid lines are exponential fits of the decays, and the inset shows the partial FT traces at three typical delays, when the center of the window is at 0.45, 0.85, and 1.85 ns, respectively.

sample. This signal contains a superposition of several echoes with a similar shape and different intensities. Because of the free surfaces at both sides of the structures, all of the acoustic energy is reflected towards the substrate and propagates back and forth several times in the whole sample. The pulse arrival at the detector surface takes place at regular times $(2n + 1)T$, where $T \cong 68$ ns is the propagation time through the whole GaAs substrate thickness. These echoes are folded back into a 12 ns time window, which is the repetition time of the femtosecond laser. Moreover, each echo appears twice due to the nonequivalence of the two arms of the Sagnac interferometer. We show in the inset in Fig. 3(a) the time variation of the displacement during the first echo ($n = 0$). To ensure a frequency resolution compatible with the expected cavity modes broadening, we performed the Fourier transform (FT) of $B(t)$ over a time window $\tau = 3.5$ ns, as indicated in Fig. 3(a). Figure 3(b) illustrates that the arrival of additional echoes does not affect the decay curve of the cavity mode, as will be explained later.

Let us first compare the Fourier transform amplitude $F(\omega)$ of the time derivative of the experimental signals measured in samples $M$ (Fig. 4, ME) and $C$ (Fig. 4, CE) with the simulated Fourier transform of the deformation of the sample surface normalized with the relevant incoming acoustic spectrum (MT or CT). Thin layer effects in the phonon generation spectrum in the aluminum layer and nonlinear propagation in the 325 $\mu$m thick GaAs substrate, cooled down at 15 K, have been taken into account to simulate the spectral shape of the actual spectrum impinging on the phonon device. Changing the excitation power density [13] modifies the slowly varying envelope in $F(\omega)$ but does not affect the rapid variations due to the device transmission. The overall correspondence in the transmission structures is remarkable, including the observation of three gaps around 0.05, 0.1, and 0.15 THz in the mirror $M$. The same gaps are observed in cavity $C$ together with additional narrow cavity modes. Because the building blocks of the mirrors are $(3\lambda_1/4, \lambda_2/4)$, the cavity mode appears at the center of the second gap while the modes in the first and third stop bands are down-shifted (respectively, up-shifted) with respect to the stop-band center. In the theoretical traces in Fig. 4, we have used the layer thicknesses independently determined by x-Ray diffraction, standard values for the acoustic parameters, and a $-0.5\%$ correction to all thicknesses to reproduce the cavity mode frequency around 100 GHz. We left apart the small remaining differences in the detail of the transmission oscillations outside the gaps, not visible at the scale in Fig. 4, as they do not affect the conclusions of the present Letter. The spectral width $\Delta f$ (FWHM) of the cavity peaks, which reflects the lifetime of phonons in the cavity, amounts to 0.43 GHz, in close agreement with the 0.32 GHz value expected from the model. We also performed partial Fourier transforms over 500 ps wide time windows centered at regularly spaced delays. We show in Fig. 3(b) the variation as a function of the delay of the heights of the cavity peak and the peak at the low energy edge of the stop band in the partial Fourier transform amplitudes. We illustrate in the inset partial FT curves at a few significant delays. Besides oscillations due to the numerical sampling, regular decays are observed and no accident is visible at the arrival of new echoes. The cavity peak displays a decay time of 1.38 ns, in excellent agreement with the value deduced from $\Delta f$ ($\tau = \sqrt{3}/\pi\Delta f = 1.28$ ns) while the edge mode decays within 0.26 ns.

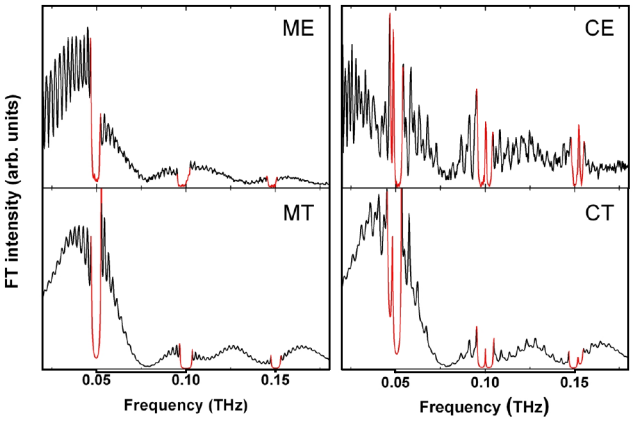


FIG. 4 (color online). Fourier transform amplitudes of the time derivative of the transient reflectivity signal ($E$) for both samples $M$ (left side) and $C$ (right side) compared to the respective calculated Fourier transform of the deformations at the surface ($T$), including the simulated incident phonon pulse spectrum. The energy range of the phonon stop bands are emphasized in red.

A definitive advantage of picosecond acoustics with respect to light transmission spectroscopy is that the transmission curve is actually obtained from a signal that contains intrinsically more information, i.e., the coherent time evolution of the wave packet. In other words, the phase $\phi$ of the transmission is also available and gives access to important quantities such as the group transit time $t_G = L/v_G$ associated to the transit of the sound pulse through the acoustic device, where $L$ is the total length of the device and $v_G$ is the group velocity. The correct definition of this basic quantity in highly dispersive media has been much debated following the initial work by Brillouin [14]. Experiments in the megahertz range have clearly demonstrated that this quantity remains meaningful in such a situation [15] and can be alternatively determined either from the basic definition $t_G(\omega) = L/(d\omega/dk) = d\phi(\omega)/d\omega$ or from numerically filtering the data. Because the latter method is less affected by experimental noise, we used it to quantify the time evolution in the studied nanocavity. We compare in Fig. 5 the experimental and the theoretical transit times through the acoustic device deduced with the same filtering procedure as introduced in Ref. [15], using a 0.01 GHz Gaussian filter. We also show as a dotted line the

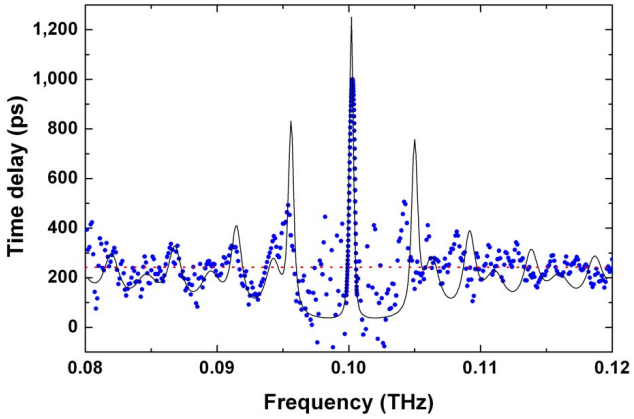


FIG. 5 (color online). Group transit time deduced from numerical filtering of the signal on sample *C* with Gaussian filters centered at various energies and with widths of 0.01 GHz (blue points). A constant time offset has been adjusted to fit the theoretical group transit time through the cavity device obtained with the same method (black line). The red dotted line shows the transit time calculated using an effective velocity as described in the text.

reference transit time $\sum d_i/v_i$. The agreement is excellent apart from some dephasing in the transmission oscillations on the high energy side of the stop band. As we already explained for Fig. 4, we have not performed a full adjustment of the sample parameters to improve the agreement in a frequency range which is not essential for the cavity behavior studied in this Letter. In the stop band, picosecond transit times, shorter than in any of the constituting materials, are observed, though with a large noise due to the very low transmission rate in the stop bands. On the other hand, transit times up to 1 ns are measured at the cavity peaks, reflecting the strong confinement of resonant phonons within the cavity layer. The very short transit times in the stop bands are an acoustic equivalent of what is known as the ''Hartman'' effect of electron tunneling through potential barriers [16]. When analyzed in the context of light propagation, this same phenomenon leads to much debated consequences, in view of the fact that light velocities above $c$ have been deduced from indirect measurements [11]. Here, in the framework of subterahertz acoustics, we have the advantage that direct observations in the time domain become accessible. On the other hand, the long lifetime of the cavity mode is clearly demonstrated in this figure. This result is similar to what is observed in photonic microcavities, an effect that is at the basis of modifications of the angular distribution of the emitted light and of the emission rate, for optical emitters such as excitons embedded in the cavities.

The results presented in this Letter fully validate the concept of the phonon nanocavity and open new ways to manipulate acoustic phonons in the technologically challenging subterahertz energy range going from high resolution filtering to generating directional monochromatic coherent or incoherent phonon beams. Phonon nanocavities also provide novel potentialities in the long-studied phonon ''laser'' problem [17], with the realization of longitudinally monomode cavities and the easy control, based on the number of Bragg pairs in the mirror, of the rate of tunneling of cavity phonons, and, hence, of radiated energy, to the outside world. Drawing a parallel with optical microcavities, one can furthermore foresee the possibility of using such cavities to modify the way in which sound interacts with electrons or with other phonons with a significant impact on electronic and optoelectronic devices.

We thank J. Page, S. Longhi, and F. Perez for useful scientific discussions and ECOS*Sud* for financial support.

[1] H. Rücker, E. Molinari, and P. Lugli, Phys. Rev. B **45**, 6747 (1992).
[2] M. Trigo, A. Bruchhausen, A. Fainstein, B. Jusserand, and V. Thierry-Mieg, Phys. Rev. Lett. **89**, 227402 (2002).
[3] V. Narayanamurti, H. L. Störmer, M. A. Chin, A. C. Gossard, and W. Wiegmann, Phys. Rev. Lett. **43**, 2012 (1979).
[4] W. M. Robertson, C. Baker, and C. Brad Bennett, Am. J. Phys. **72**, 255 (2004).
[5] F. R. Montero de Espinosa, E. Jiménez, and M. Torres, Phys. Rev. Lett. **80**, 1208 (1998).
[6] Yang Suxia, J. H. Page, Liu Zhengyou, M. L. Cowan, C. T. Chan, and Ping Sheng, Phys. Rev. Lett. **88**, 104301 (2002).
[7] F. Van Der Biest, A. Sukhovich, A. Tourin, J. H. Page, B. A. van Tiggelen, Z. Liu, and M. Fink, Europhys. Lett. **71**, 63 (2005).
[8] N. M. Stanton, R. N. Kini, A. J. Kent, M. Henini, and D. Lehmann, Phys. Rev. B **68**, 113302 (2003).
[9] H. Maris, Sci. Am. **278**, No. 1, 64 (1998).
[10] B. Perrin, B. Bonello, J.-C. Jeannet, and E. Romatet, Physica (Amsterdam) **219B–220B**, 681 (1996).
[11] S. Longhi, P. Laporta, M. Belmonte, and E. Recami, Phys. Rev. E **65**, 046610 (2002).
[12] J.-Y. Duquesne and B. Perrin, Phys. Rev. B **68**, 134205 (2003).
[13] E. Peronne and B. Perrin, Ultrasonics (to be published).
[14] L. Brillouin, *Wave Propagation and Group Velocity* (Academic, New York, 1960).
[15] J. H. Page, Ping Sheng, H. P. Schriemer, I. Jones, Xiaodun Jing, and D. A. Weitz, Science **271**, 634 (1996).
[16] T. E. Hartman, J. Appl. Phys. **33**, 3427 (1962).
[17] P. A. Fokker, J. I. Dijkhuis, and H. W. de Wijn, Phys. Rev. B **55**, 2925 (1997).